Gromov–Wasserstein Problem with Cyclic Symmetry

Appendix

Shoichiro Takeda Yasunori Akagi
NTT Corporation
{shoichiro.takeda, yasunori.akagi}@ntt.com

A. Proof of Lemma 1

We can explicitly write $\mathbf{Q}$ under Assumption 1 as follows;

$$\begin{aligned}
\mathbf{Q} &= \mathbf{C}^{\circ 2}\mathbf{a}\mathbf{1}_n^\top + \mathbf{1}_m\mathbf{b}^\top(\mathbf{D}^{\circ 2})^\top \\
&= \begin{pmatrix} \mathbf{C}_0^{\circ 2} & \mathbf{C}_1^{\circ 2} & \cdots & \mathbf{C}_{K-1}^{\circ 2} \\ \mathbf{C}_{K-1}^{\circ 2} & \mathbf{C}_0^{\circ 2} & \ddots & \vdots \\ \vdots & \ddots & \ddots & \mathbf{C}_1^{\circ 2} \\ \mathbf{C}_1^{\circ 2} & \cdots & \mathbf{C}_{K-1}^{\circ 2} & \mathbf{C}_0^{\circ 2} \end{pmatrix} \begin{pmatrix} \boldsymbol{\alpha}\mathbf{1}_{n'}^\top & \boldsymbol{\alpha}\mathbf{1}_{n'}^\top & \cdots & \boldsymbol{\alpha}\mathbf{1}_{n'}^\top \\ \boldsymbol{\alpha}\mathbf{1}_{n'}^\top & \boldsymbol{\alpha}\mathbf{1}_{n'}^\top & \ddots & \vdots \\ \vdots & \ddots & \ddots & \boldsymbol{\alpha}\mathbf{1}_{n'}^\top \\ \boldsymbol{\alpha}\mathbf{1}_{n'}^\top & \cdots & \boldsymbol{\alpha}\mathbf{1}_{n'}^\top & \boldsymbol{\alpha}\mathbf{1}_{n'}^\top \end{pmatrix} \\
&\quad + \begin{pmatrix} \mathbf{1}_{m'}\boldsymbol{\beta}^\top & \mathbf{1}_{m'}\boldsymbol{\beta}^\top & \cdots & \mathbf{1}_{m'}\boldsymbol{\beta}^\top \\ \mathbf{1}_{m'}\boldsymbol{\beta}^\top & \mathbf{1}_{m'}\boldsymbol{\beta}^\top & \ddots & \vdots \\ \vdots & \ddots & \ddots & \mathbf{1}_{m'}\boldsymbol{\beta}^\top \\ \mathbf{1}_{m'}\boldsymbol{\beta}^\top & \cdots & \mathbf{1}_{m'}\boldsymbol{\beta}^\top & \mathbf{1}_{m'}\boldsymbol{\beta}^\top \end{pmatrix} \begin{pmatrix} \mathbf{D}_0^{\circ 2} & \mathbf{D}_1^{\circ 2} & \cdots & \mathbf{D}_{K-1}^{\circ 2} \\ \mathbf{D}_{K-1}^{\circ 2} & \mathbf{D}_0^{\circ 2} & \ddots & \vdots \\ \vdots & \ddots & \ddots & \mathbf{D}_1^{\circ 2} \\ \mathbf{D}_1^{\circ 2} & \cdots & \mathbf{C}_{K-1}^{\circ 2} & \mathbf{D}_0^{\circ 2} \end{pmatrix} \\
&= \begin{pmatrix} \widehat{\mathbf{Q}} & \widehat{\mathbf{Q}} & \cdots & \widehat{\mathbf{Q}} \\ \widehat{\mathbf{Q}} & \widehat{\mathbf{Q}} & \ddots & \vdots \\ \vdots & \ddots & \ddots & \widehat{\mathbf{Q}} \\ \widehat{\mathbf{Q}} & \cdots & \widehat{\mathbf{Q}} & \widehat{\mathbf{Q}} \end{pmatrix},
\end{aligned}$$

where $\widehat{\mathbf{Q}} \coloneqq \sum_{i=0}^{K-1} \mathbf{C}_i^{\circ 2}\boldsymbol{\alpha}\mathbf{1}_{n'}^\top + \mathbf{1}_{m'}\boldsymbol{\beta}^\top(\mathbf{D}_i^{\circ 2})^\top$.

B. Proof of Theorem 1

Because $\mathbf{C}, \mathbf{D}, \mathbf{T}^{(\tau)}$, and $\mathbf{Q}$ are (m', n', K)-block circulant matrices and the set of (m', n', K)-block circulant matrices is closed under addition, subtraction, matrix product, and transposition, $\mathbf{G}^{(\tau)}$ given by (3) is an (m', n', K)-block circulant matrix.

Similarly, because the set of (m', n', K)-block circulant matrices is closed under addition and scalar product, $\mathbf{T}^{(\tau+1)}$ given by (5) is an (m', n', K)-block circulant matrix when $\mathbf{S}^{(\tau)}$ is an (m', n', K)-block circulant matrix.

We next show the existence of an (m', n', K)-block circulant matrix which is an optimal solution to the problem (4). Let $\mathbf{S}'$ be an optimal solution to (4). We define $\mathbf{S}^*$ as follows:

$$\mathbf{S}^* \coloneqq \frac{1}{K}\sum_{k=0}^{K-1} \mathbf{P}^k \mathbf{S}' \left(\mathbf{P}^k\right)^\top,$$

where

$$\mathbf{P}^k \coloneqq \begin{pmatrix} \mathbf{0}_{K-1} & \mathbf{I}_{K-1} \\ 1 & \mathbf{0}_{K-1}^\top \end{pmatrix}^k \otimes \mathbf{I}_{m' \times n'}.$$

Then, we get

$$\mathbf{S}^*\mathbf{1}_n = \frac{1}{K}\sum_{k=0}^{K-1} \mathbf{P}^k \mathbf{S}' \left(\mathbf{P}^k\right)^\top \mathbf{1}_n = \frac{1}{K}\sum_{k=0}^{K-1} \mathbf{P}^k \mathbf{S}' \mathbf{1}_n = \frac{1}{K}\sum_{k=0}^{K-1} \mathbf{P}^k \mathbf{a} = \frac{1}{K}\sum_{k=0}^{K-1} \mathbf{a} = \mathbf{a}.$$

and $(\mathbf{S}^*)^\top \mathbf{1}_m = \mathbf{b}$ by similar calculation. Because obviously $\mathbf{S}^* \in \mathbb{R}_{\geq 0}^{m \times n}$, $\mathbf{S}^*$ is a feasible solution to (4), *i.e.*, $\mathbf{S}^* \in \Pi(\mathbf{a}, \mathbf{b}) = \{\mathbf{X} \in \mathbb{R}_{\geq 0}^{m \times n} \mid \mathbf{X}\mathbf{1}_n = \mathbf{a}, \mathbf{X}^\top \mathbf{1}_m = \mathbf{b}\}$.

Next we check the objective function value. Let $f^{(\tau)}(\mathbf{S})$ be the objective function of (4). We get

$$f^{(\tau)}(\mathbf{S}^*) = f^{(\tau)}\left(\frac{1}{K}\sum_{k=0}^{K-1} \mathbf{P}^k \mathbf{S}' \left(\mathbf{P}^k\right)^\top\right) \leq \frac{1}{K}\sum_{k=0}^{K-1} f^{(\tau)}\left(\mathbf{P}^k \mathbf{S}' \left(\mathbf{P}^k\right)^\top\right) = \frac{1}{K}\sum_{k=0}^{K-1} f^{(\tau)}(\mathbf{S}') = f^{(\tau)}(\mathbf{S}'). \tag{A1}$$

Note that we use the convexity of $f^{(\tau)}$ and Jensen's inequality in the inequality relationship of the above equation. The inequality (A1) and the optimality of $\mathbf{S}'$ to (4) indicates that $\mathbf{S}^*$ is also an optimal solution to (4).

Finally, because

$$\mathbf{P}^l \mathbf{S}^* (\mathbf{P}^l)^\top = \frac{1}{K}\sum_{k=0}^{K-1} \mathbf{P}^{k+l} \mathbf{S}' (\mathbf{P}^{k+l})^\top = \frac{1}{K}\sum_{k=0}^{K-1} \mathbf{P}^k \mathbf{S}' (\mathbf{P}^k)^\top = \mathbf{S}^*$$

holds for $l = 0, \ldots, K-1$, $\mathbf{S}^*$ is an (m', n', K)-block circulant matrix.

C. Synthetic 2D Point Sets

In Secs. 6.1 and 6.2, we generated synthetic 2D point sets for validating the effectiveness of our algorithms. We here show how to generate them for details. We first generated a 2D point set $\mathcal{D}^0$ as follows.

$$\mathcal{D}^0 \coloneqq \left\{ (x_i, y_i) = (r_i \cos\theta_i, r_i \sin\theta_i) \;\middle|\; r_i \sim \mathrm{U}(0,1),\ \theta_i \sim \mathrm{U}\left(0, \frac{2\pi}{K}\right),\ i = 0, \ldots, \frac{d}{K} \right\},$$

where $\mathrm{U}(a, b)$ denotes the uniform distribution between $[a, b)$. Then, we duplicated the 2D point set with rotation as

$$\mathcal{D}^k \coloneqq \left\{ (x_i, y_i)\mathbf{R}_K^k \;\middle|\; (x_i, y_i) \in \mathcal{D}^0 \right\},$$

for $k = 1, \ldots, K-1$, where

$$\mathbf{R}_K^k \coloneqq \begin{pmatrix} \cos\frac{2\pi k}{K} & \sin\frac{2\pi k}{K} \\ -\sin\frac{2\pi k}{K} & \cos\frac{2\pi k}{K} \end{pmatrix}$$

is a transposed 2D rotation matrix that rotates 2D points (x_i, y_i) counterclockwise by the angle $\frac{2\pi k}{K}$. Finally, we united the all 2D point sets $\mathcal{D}^0, \mathcal{D}^1, \ldots, \mathcal{D}^{K-1}$ into the one 2D point set $\mathcal{D}$ as follows.

$$\mathcal{D} \coloneqq \bigcup_{k=0}^{K-1} \mathcal{D}^k$$

This 2D point set $\mathcal{D}$ exhibits K-order rotational symmetry on a 2D plane.

D. Symmetric Alignment for Vertices of 2D Objects

In Sec. 6.3, for the input data to C-CG and C-SP, we aligned the vertices of each 2D object to exhibit strict mirror symmetry. Let $\mathcal{V} \coloneqq \{(x_i, y_i) \in \mathbb{R}^2 \mid i = 0, \ldots, d-1\}$ be the vertices of each 2D object which have a mean of zero. We first detected the mirror symmetric line using the first (or second) principal component vector (x_p, y_p) obtained by the principal component analysis (PCA). The mirror symmetric line can be written as the the line equation $y - \frac{y_p}{x_p}x = 0$. Then, we chose the vertices on one side of the mirror symmetric line as follows.

$$\mathcal{W} \coloneqq \left\{ (x_i, y_i) \in \mathcal{V} \;\middle|\; y_i - \frac{y_p}{x_p}x_i \geq 0 \right\}.$$

After that, we obtained the reflection of $\mathcal{W}$ across the mirror symmetric line as follows.

$$\mathcal{W}_{\text{ref}} \coloneqq \left\{ 2(\hat{x}_i, \hat{y}_i) - (x_i, y_i) \mid (x_i, y_i) \in \mathcal{W} \right\},$$

where $(\hat{x}_i, \hat{y}_i)$ is the projection point of (x_i, y_i) onto the mirror symmetric line given by

$$(\hat{x}_i, \hat{y}_i) = \left(\frac{x_i x_p + y_i y_p}{x_p^2 + y_p^2} x_p, \frac{x_i x_p + y_i y_p}{x_p^2 + y_p^2} y_p \right).$$

Finally, we obtained the symmetrically aligned vertices $\mathcal{V}_{\text{sym}}$ by uniting $\mathcal{W}$ and $\mathcal{W}_{\text{ref}}$ as $\mathcal{V}_{\text{sym}} = \mathcal{W} \cup \mathcal{W}_{\text{ref}}$. Note that if we obtain $x_p = 0$, we can obtain $\mathcal{V}_{\text{sym}}$ by a similar process with $\mathcal{W} \coloneqq \{(x_i, y_i) \in \mathcal{V} \mid x_i \geq 0\}$.

E. Further Analysis in Sec. 6.3

In Sec. 6.3, C-CG showed better results than CG with or without the symmetric alignment. Figure A1 shows the coupling between 2D object examples using each algorithm in Sec. 6.3. As you can see, our C-CG considers the cyclic symmetry of input data and thus obtained a coupling from the right part of the source object (blue) to the right part of the target object (red), which results in a lower GWD (*i.e.*, a better local solution) than CG with or without the symmetric alignment. Note that we observed the equally optimal couplings crossing the mirror symmetry and here showed no-crossing examples. In contrast, CG with or without the symmetric alignment did not consider the cyclic symmetry of input data explicitly and thus obtained an unreasonable coupling from the right part of the source object to the left irrelevant parts of the target object across the symmetric center line, which results in higher GWDs (*i.e.*, worse local solutions) than C-CG. This trend was also observed among SP, SP with the symmetric alignment, and C-SP.

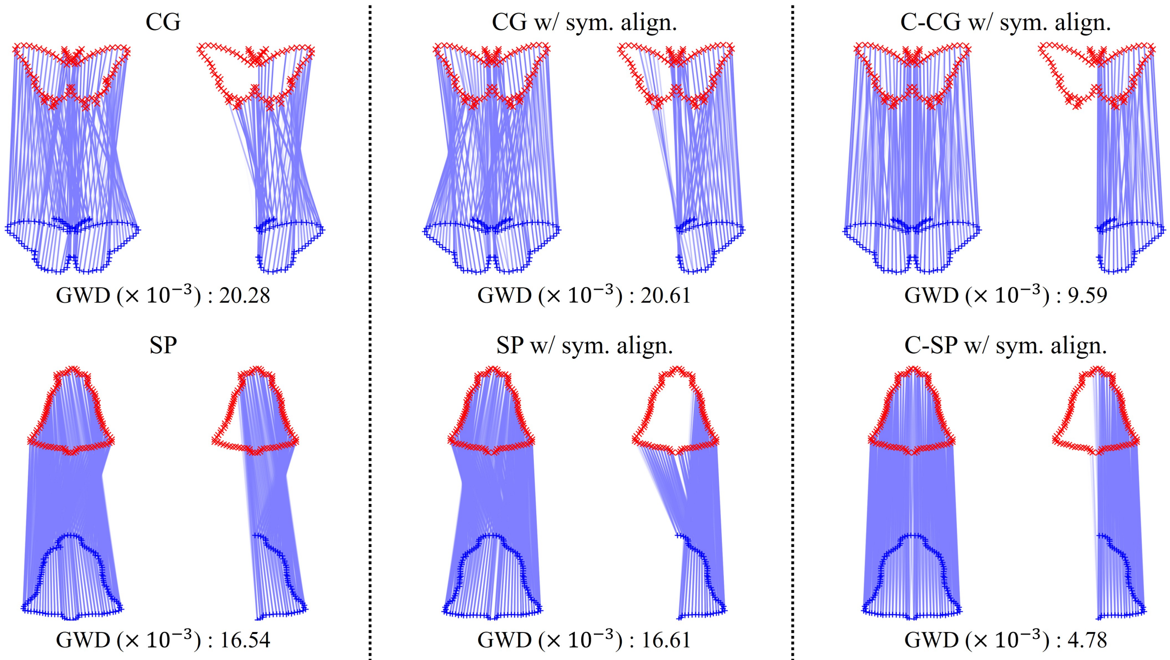

Figure A1. The coupling between 2D object examples using each algorithm in Sec. 6.3. In each algorithm, the left panel shows the whole coupling between the two objects, and the right panel shows the coupling from half of the source object (blue) to the target object (red).

F. Symmetric Alignment for 3D Point Cloud

In Sec. 6.4, for the input data to C-CG and C-SP, we aligned the point cloud of each 3D object to exhibit strict mirror symmetry. Let $\mathcal{V} \coloneqq \{(x_i, y_i, z_i) \in \mathbb{R}^3 \mid i = 0, \ldots, d-1\}$ be the points of each point cloud which have a mean of zero. The dataset used in Sec. 6.4 is well-maintained, and 3D objects are arranged to be mirror symmetric with respect to the YZ-axes plane. Thus, we chose the points on one side of the mirror symmetric plane as follows.

$$\mathcal{W} \coloneqq \{(x_i, y_i, z_i) \in \mathcal{V} \mid x_i \geq 0\}.$$

After that, we obtained the reflection of $\mathcal{W}$ across the mirror symmetric plane as follows.

$$\mathcal{W}_{\text{ref}} \coloneqq \{(-x_i, y_i, z_i) \mid (x_i, y_i, z_i) \in \mathcal{W}\}.$$

Finally, we obtained the symmetrically aligned point cloud $\mathcal{V}_{\text{sym}}$ by uniting $\mathcal{W}$ and $\mathcal{W}_{\text{ref}}$ as $\mathcal{V}_{\text{sym}} = \mathcal{W} \cup \mathcal{W}_{\text{ref}}$.

G. On the Optimal Solution to C-EGW

As explained in Sec. 5.1, the outputs of the proposed algorithms, C-CG and C-PG, are restricted to (m', n', K)-block circulant matrices. This raises the following question: Does a (m', n', K)-block circulant matrix always exist as a globally optimal solution to C-EGW? The following proposition shows that this is not necessarily the case.

Proposition A1. There exists an instance of C-EGW whose globally optimal solution is not an (m', n', K)-block circulant matrix.

Proof. We consider the case where $(m, n, K, \varepsilon) = (4, 4, 2, 0)$. Let

$$\mathbf{a} = \begin{pmatrix} \frac{1}{4} & \frac{1}{4} & \frac{1}{4} & \frac{1}{4} \end{pmatrix}^\top, \quad \mathbf{b} = \begin{pmatrix} \frac{1}{4} & \frac{1}{4} & \frac{1}{4} & \frac{1}{4} \end{pmatrix}^\top, \quad \mathbf{C} = \begin{pmatrix} 0 & 0 & 1 & 0 \\ 0 & 0 & 0 & 0 \\ 1 & 0 & 0 & 0 \\ 0 & 0 & 0 & 0 \end{pmatrix}, \quad \mathbf{D} = \begin{pmatrix} 0 & 0 & 0 & 1 \\ 0 & 0 & 0 & 0 \\ 0 & 1 & 0 & 0 \\ 0 & 0 & 0 & 0 \end{pmatrix}.$$

Any $(2, 2, 2)$-block circulant matrix can be written as

$$\mathbf{T} = \begin{pmatrix} a & b & e & f \\ c & d & g & h \\ e & f & a & b \\ g & h & c & d \end{pmatrix}.$$

Then, the objective function value of C-EGW can be calculated as follows:

$$\begin{aligned} \sum_{i,i',j,j'} (C_{ii'} - D_{jj'})^2 T_{ij} T_{i'j'} &= \frac{1}{4} - 4ab - 4ef \\ &\geq \frac{1}{4} - (a+b)^2 - (e+f)^2 \\ &= \frac{1}{4} - (a+b)^2 - \left(\frac{1}{4} - (a+b)\right)^2 \qquad \left(\because \text{the row sum constraint: } a+b+e+f = \frac{1}{4}\right) \\ &= \frac{7}{32} - 2\left(a + b - \frac{1}{8}\right)^2 \geq \frac{3}{16}. \qquad \left(\because 0 \leq a+b \leq \frac{1}{4}\right) \end{aligned}$$

On the other hand, when

$$\mathbf{T} = \begin{pmatrix} 0 & \frac{1}{4} & 0 & 0 \\ \frac{1}{10} & 0 & 0 & \frac{3}{20} \\ 0 & 0 & \frac{1}{4} & 0 \\ \frac{3}{20} & 0 & 0 & \frac{1}{10} \end{pmatrix},$$

the objective function value of C-EGW is $\frac{3}{25}$, which is smaller than $\frac{3}{16}$. This implies that a $(2, 2, 2)$-block circulant matrix can never be a globally optimal solution to this instance of C-EGW. $\square$

Proposition A1 highlights a limitation of this study, showing that there exists an instance of C-EGW to which the proposed algorithms can never yield a globally optimal solution. This limitation stems from the non-convexity of the GW objective function and does not occur in standard OT, which is a convex optimization problem.

H. Performance Analysis using Naive Symmetric-Aware Approach

For a further fair comparison, we here tested a naive symmetry-aware approach in the same setting of Sec. 6.1, which considers only one of the symmetric parts of input data. Specifically, this naive approach first solved GW or EGW for the input data $\boldsymbol{\alpha}, \boldsymbol{\beta}, \mathbf{C}_0$ and $\mathbf{D}_0$, and then duplicated the obtained solution $\mathbf{T}_0$ K times as $\mathbf{T} = \mathbf{I}_K \otimes \mathbf{T}_0$ for all symmetric parts. In this naive approach, we used CG or SP to solve GW or EGW and referred to them as naive CG (N-CG) or naive SP (N-SP), respectively. As an initial solution for N-CG or N-SP, we created a uniform random matrix in $[0, 1)^{m' \times n'}$ and scaled it to lie within $\Pi'(\boldsymbol{\alpha}, \boldsymbol{\beta})$ using the Sinkhorn-Knopp algorithm.

Table A1 showed the results. N-CG and N-SP deteriorated GWDs so much compared to other algorithms in Tab. 1 because they did not consider the cyclic symmetry of input data properly and completely ignored the couplings between the symmetric parts. The deterioration was more severe when a larger K value was used because using a larger K value in N-CG or N-SP increasingly ignores the couplings between the symmetric parts.

Algo.	K	GWD $(\times 10^{-3})$	# of iterations	Time (s)
N-CG	2	26.79 ± 54.10	12.41 ± 4.92	2.67 ± 0.99
	5	112.07 ± 115.91	9.45 ± 4.97	0.22 ± 0.10
	10	171.86 ± 156.70	4.95 ± 1.16	0.03 ± 0.01
N-PG	2	12.74 ± 3.52	6.97 ± 1.92	0.59 ± 0.19
	5	47.33 ± 22.3	8.65 ± 1.34	0.11 ± 0.02
	10	91.93 ± 112.25	6.54 ± 0.89	0.03 ± 0.01

Table A1. Performance analysis with synthetic data as in Section 6.1 using the naive symmetry-aware approach explained in H. "Algo." means "Algorithm." Mean $\pm$ SD is shown in each result. # means "the number." "s" is the symbol for seconds.

I. Performance Analysis under Data-Swapping Disturbance

Given data with cyclic symmetry, there is some arbitrariness in selecting symmetric points. In this experiment, we evaluated the effect of data swapping on our algorithms. Specifically, we randomly swapped corresponding symmetric points based on a given swapping ratio, while preserving the cyclic symmetry of the input data. We tested C-CG and C-PG using 10 different initial solutions for the point cloud data with mirror symmetry in Fig. 2.

Table A2 shows the results. C-CG for solving C-GW showed larger GWDs as the larger swapping ratio. This is because the swapping increases each value in the Euclidean distance matrices ($\mathbf{C}$ and $\mathbf{D}$) and amplifies the GWD value larger when a bad local solution is reached. In contrast, C-PG for solving C-EGW showed almost the same GWDs in all cases. This implies that adding the entropy regularization allows the solution space to be non-sparse and softer, which efficiently avoids bad local solutions and obtains robustness against the data-swapping fluctuations.

Algo.	Swap (%)	GWD $(\times 10^{-3})$	# of iterations	Time (s)
C-CG	0	2.388 ± 1.633	5.3 ± 0.458	1.750 ± 0.181
	25	3.204 ± 2.000	5.4 ± 0.490	1.783 ± 0.195
	50	4.428 ± 1.870	6.1 ± 1.375	2.013 ± 0.473
C-PG	0	3.104 ± 0.000	7.3 ± 0.458	1.094 ± 0.083
	25	3.104 ± 0.001	7.1 ± 0.300	1.054 ± 0.061
	50	3.105 ± 0.001	7.2 ± 0.400	1.061 ± 0.075

Table A2. The effects of data swapping that preserves cyclic symmetry of input data. "Swap" means the swapping ratio.